

A cluster of young stellar objects in L1211

M. Tafalla¹, P.C. Myers², D. Mardones³, and R. Bachiller¹

¹ Observatorio Astronómico Nacional, Apartado 1143, E-28800 Alcalá de Henares, Spain (tafalla, bachiller@oan.es)

² Harvard-Smithsonian Center for Astrophysics, MS 42, 60 Garden St., Cambridge, MA 02138, USA (pmyers@cfa.harvard.edu)

³ Departamento de Astronomía, Universidad de Chile, Casilla 36-D, Santiago, Chile (mardones@das.uchile.cl)

Received 19 February 1999 / Accepted 28 May 1999

Abstract. We present millimeter continuum and line observations of a dense core in L1211, a member of the Cepheus cloud complex. We find a small cluster of at least 4 millimeter (mm) sources with no optical counterpart, but each associated with near infrared (NIR) diffuse emission. The strongest mm source has no NIR point-like counterpart, and constitutes a good candidate for a Class 0 object. The other mm objects seem associated with NIR sources and most likely belong to Class I, as also suggested by the spectral energy distributions derived from combining our mm data with IRAS HIRES fluxes. As evidenced by our line data, the mm sources are embedded in an elongated, turbulent core of about $150 M_{\odot}$ of mass and 0.6 pc length. Two of the millimeter sources power bipolar molecular outflows, another signature of their extreme youth. The outflows are well resolved by our observations and seem to have unrelated orientations.

The combination of millimeter sources and bipolar outflow emission indicates that multiple star formation in L1211 has occurred during a short period of time (a few 10^5 yr). The lack of a noticeable enhancement in the number of NIR sources suggests that the core has not had enough time to form a cluster, so we infer that L1211 is undergoing a first episode of star formation.

Key words: stars: formation – ISM: clouds – ISM: dust, extinction – ISM: individual objects: L1211 – ISM: jets and outflows – ISM: molecules

1. Introduction

L1211 is a class 5 dark cloud (Lynds 1962) about 1° west of Cepheus A. Its angular proximity to the group of Cepheus A-F clouds (mapped by Sargent 1977, 1979, Yu et al. 1996, and Yonekura et al. 1997) and its similar LSR velocity (Yu et al. 1996, this work) suggest that it is related to the group, and therefore lies at a similar distance from the Sun (725 pc, see Crawford & Barnes 1970, Sargent 1977). In contrast with the Cepheus group of clouds, not much is known about L1211. Fukui (1989) has reported a bipolar outflow around the embedded source IRAS 22453+6146, although no map of the accelerated gas has been published so far. Harju et al. (1993) have mapped the ammonia emission around this source, finding a

dense molecular core, and Hodapp (1994) has imaged the region in K' ($2.1 \mu\text{m}$) as part of an outflow survey, finding several sources associated with diffuse emission and classifying the system as a small cluster.

During a 1.2 mm continuum search for embedded objects in nearby, very young NIR groups associated with outflows, we found that IRAS 22453+6146 was unusual. Most sources in our sample (selected from the images of Hodapp 1994) have only one compact millimeter counterpart, despite having multiple IR sources. L1211, on the other hand, has at least 4 well-separated mm sources, suggesting that star formation in the cloud has occurred in a different manner, probably more efficiently or in a synchronized way. For this reason, we have investigated L1211 in more detail, following the 1.2 mm continuum observations with molecular line mapping to characterize the core and determine the distribution of high velocity gas. In this paper, we report the results from this combined study.

2. Observations

We observed L1211 in the mm continuum using the MPIfR 19-element bolometer array on the IRAM 30 m telescope in 1997 February. The bolometer operates at a central wavelength of 1.2 mm (240 GHz) and has a bandwidth of 70 GHz (Kreysa 1992, Guélin et al. 1995). The observations were done on the fly, scanning in azimuth at a rate of $4'' \text{ sec}^{-1}$ with a wobbler throw of $41''$ and a period of 0.5 sec. The atmospheric optical depth correction was estimated from sky dips done before and after the source mapping, and applied to the data, which were fully reduced with the NIC software (Brogière et al. 1998). Pointing corrections were measured immediately before observing L1211 by making cross scans on 2200+420 (BL Lac), and source pointing accuracy is estimated to be better than $3''$. Two maps were made in two different days and later combined, achieving an rms sensitivity at the image center of about 7 mJy beam^{-1} . Based on Uranus observations, the beam FWHM was approximately $11''$.

Having found multiple 1.2 mm sources in L1211, we went back to the IRAM 30m telescope in 1997 August to observe the molecular gas in the lines of $^{12}\text{CO}(J=1-0)$, $^{12}\text{CO}(2-1)$, $\text{CS}(2-1)$, $\text{CS}(3-2)$, and $\text{C}^{18}\text{O}(2-1)$. The observations were done with two receiver configurations. The first one, to map the outflow

Send offprint requests to: M. Tafalla

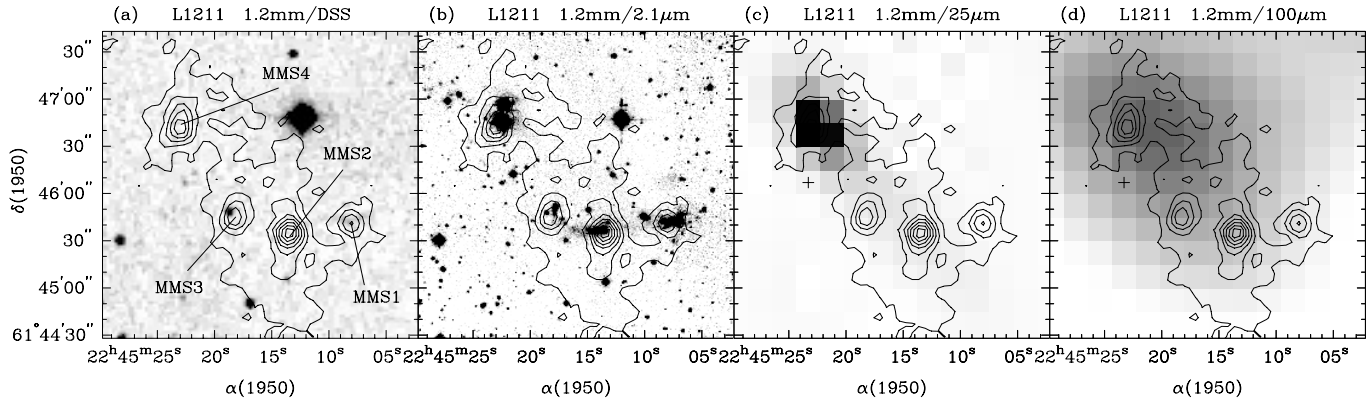


Fig. 1a–d. Distribution of 1.2 mm emission (contours) superposed to images of emission at different wavelengths. **a** Optical DSS (red) image. **b** K' ($2.1 \mu\text{m}$) image from Hodapp (1994). **c** $25 \mu\text{m}$ IRAS HIRES image. **d** $100 \mu\text{m}$ IRAS HIRES image. Absolute coordinates for the K' image (larger than shown) were estimated from the coordinates in the DSS image by identifying three common stars and calculating a linear transfer function between pixels in the K' image and equatorial coordinates in the DSS image. Comparing the alignment of additional stars common to both images, we estimate the coordinates in the K' image are accurate within $2''$. Contours are at intervals of 25 mJy per $11''$ beam starting at 25 mJy per $11''$ beam, and the small cross in the right panels indicates the PSC position of IRAS 22453+6146. The beam size (FWHM) for the 1.2 mm data is $11''$, for the $25 \mu\text{m}$ IRAS HIRES image is $50'' \times 30''$ (PA 20°), and for the $100 \mu\text{m}$ IRAS HIRES image is $115'' \times 105''$ (PA 20°).

emission, used simultaneously four receivers tuned to both polarizations of $^{12}\text{CO}(1-0)$ and $^{12}\text{CO}(2-1)$, and position switching mode. The second configuration, to map the dense core, used three receivers simultaneously tuned to $\text{CS}(2-1)$, $\text{CS}(3-2)$, and $\text{C}^{18}\text{O}(2-1)$, and frequency switching mode. As spectrometer, we used an autocorrelator with velocity resolutions of 0.20 km s^{-1} for $^{12}\text{CO}(1-0)$, 0.40 km s^{-1} for $^{12}\text{CO}(2-1)$, 0.060 km s^{-1} for $\text{CS}(2-1)$, 0.080 km s^{-1} for $\text{CS}(3-2)$, and 0.053 km s^{-1} for $\text{C}^{18}\text{O}(2-1)$. The beam FWHM of the telescope varies linearly with wavelength, and for our observations ranges from $24''.5$ for $\text{CS}(2-1)$ to $11''$ for $^{12}\text{CO}(2-1)$ (see Wild 1995). Pointing was corrected using continuum cross scans on NGC 7538 and it is estimated to be accurate within $4''$. Antenna temperatures are given in the main beam brightness scale.

3. Results

3.1. Continuum data

Fig. 1 presents the 1.2 mm continuum emission (contours) superposed to the Digitized Sky Survey (DSS) red image, the K' band ($2.1 \mu\text{m}$) image from Hodapp (1994), and the 25 and $100 \mu\text{m}$ IRAS HIRES (20 iterations) images. (The HIRES images were generated by the Maximum Correlation Method of Aumann et al. 1990 and kindly provided by IPAC). As the maps show, the 1.2 mm emission consists of at least 4 discrete maxima connected by weak, extended emission at a level of $50 \text{ mJy } (11'' \text{ beam})^{-1}$. The discrete maxima will be referred hereafter as MMS1, MMS2, MMS3, and MMS4 in order of increasing right ascension (see leftmost panel), and estimates of their positions and fluxes are given in Table 1. The peak flux in the table is the total 1.2 mm flux at each source position, while the integrated flux is our best estimate to the intrinsic source flux, and was derived by subtracting a $50 \text{ mJy } (11'' \text{ beam})^{-1}$ background to the data and fitting the residual with 2-dimensional Gaussians.

Table 1. L1211 millimeter sources

Source	$\alpha(1950)$ h m s	$\delta(1950)$ ° ' "	Peak Flux ^a mJy/beam	Int. Flux ^b mJy	Mass ^c M_{\odot}
MMS1	22 45 08.1	61 45 41	105	45	0.3
MMS2	22 45 13.5	61 45 35	190	215	1.3
MMS3	22 45 18.2	61 45 46	125	85	0.5
MMS4	22 45 23.0	61 46 43	150	135	0.8

^a Observed peak flux with $11''$ beam

^b Integrated after background subtraction (see text)

^c Assuming optically thin dust at 30 K with an opacity of $0.01 \text{ cm}^2 \text{ g}^{-1}$

As it can be seen, individual source fluxes range from about 50 to 200 mJy.

The superposition of the mm data with the DSS (red) image (Fig. 1a) shows that none of the millimeter peaks has an optical stellar counterpart (the star toward MMS3 is probably a foreground source, see below), although MMS1 seems associated with weak east-west diffuse emission. In contrast, all mm sources are associated with diffuse $2.1 \mu\text{m}$ emission (see Fig. 1b). MMS1 coincides with a bright spot of IR emission consisting of east-west diffuse emission and possibly one or more point-like components. MMS2 also coincides with eastward diffuse (cometary) emission, but there is no evidence for a $2.1 \mu\text{m}$ point-like counterpart; all the emission is diffuse. MMS3 has as probable $2.1 \mu\text{m}$ counterpart the source with weak southern diffuse emission that lies slightly north of the mm peak, while the star about $10''$ southeast of this source is probably a foreground source, since it has no diffuse emission and is prominent on the DSS image. Finally, MMS4 seems associated with a group of at least three $2.1 \mu\text{m}$ sources, one near the mm peak and a close pair to the north, all three surrounded by extended emission. As the millimeter emission from MMS4 is elongated north-south, it is most likely associated with at least two IR sources, the one

Table 2. L1211 IRAS-HIRES and mm estimated fluxes

Source	12 μm	25 μm	60 μm	100 μm	1200 μm
	Jy	Jy	Jy	Jy	Jy
MMS1-2-3	0.11	0.75	13	14	0.35
MMS4	2.3	4.3	17	38	0.22

near the mm peak and at least one of the northern group. Our millimeter observations, therefore, show that in L1211 there are at least 4 young stellar objects in a region of approximately $120''$ in diameter (0.4 pc for an assumed distance of 725 pc).

The two right panels of Fig. 1 compare the 1.2 mm emission with the IRAS HIRES data. The nominal PSC position of IRAS 22453+6146 is indicated by a small cross sign, and clearly does not coincide with the real IR emission peak. This offset can be seen even in the unprocessed IRAS images, and probably results from the combined effect of confusion with the emission from the strong, nearby source IRAS 22451+6154 (8.5 arcminutes to the northwest) and the source multiplicity in the cluster. The HIRES data show that MMS4 is the brightest source of the group and dominates the emission at 12 and 25 μm , and is still brighter than the others (but more comparable) at 60 and 100 μm .

Despite the increase in angular resolution, the HIRES data cannot completely separate the contributions from the individual mm sources, although they allow to distinguish between emission from MMS4 and from the combined MMS1-2-3 group. To estimate the IRAS fluxes for these two components, we have fitted the HIRES data using two 2-dimensional gaussians of fixed widths equal to the HIRES beam widths, one at the position of MMS4 and the other located towards MMS2 (a full four-component fit failed). In this fitting, the source at MMS2 represents the combination of MMS1-2-3, and was chosen in that way because MMS2 looks brighter than MMS1 and MMS3 in the HIRES data and has an intermediate position. With this method, we derive the fluxes given in Table 2.

With the IRAS and the 1.2 mm fluxes, we estimate the spectral energy distributions (SEDs) for MMS4 and for the combination of MMS1-2-3. To complement our data, we use the K' image from Hodapp (1994), which unfortunately is uncalibrated, and therefore not ideal for a flux determination. For this reason, we choose to only estimate safe upper limits to the K' magnitudes of MMS1-2-3 and MMS4. Following Hodapp (1994, see his Fig. 5), the brightest source in the whole L1211 image has $K' = 10$, and the next one about 11 mag. As MMS4 is not the brightest source, we can safely assume that it is $K' = 11$ at most. Comparing the counts of MMS4 with those from MMS1 (the brightest of the 1-2-3 group), we estimate that MMS1 is at least 10 times weaker than MMS4 in K' . With these numbers, we present our best estimate of the SED in Fig. 2. Integrating the fluxes, and assuming a distance of 725 pc, we derive bolometric luminosities of $35 L_{\odot}$ for MMS4 and $12 L_{\odot}$ for the combination of MMS1-2-3.

As Fig. 2 shows, the SED of MMS4 is rather flat and slightly increasing redward of 100 μm , while that of MMS1-2-3 is nar-

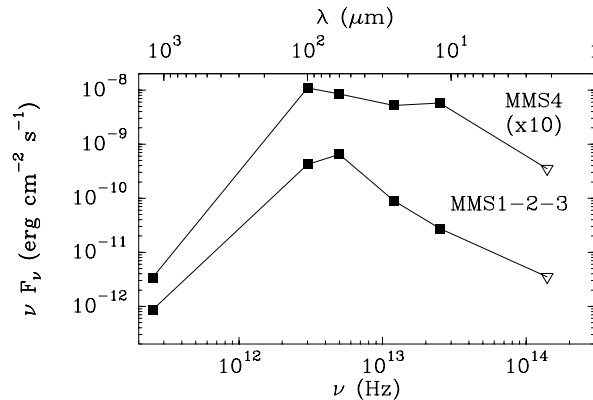


Fig. 2. Spectral energy distributions of L1211-MMS4 and combination of L1211-MMS1, MMS2, and MMS3 (not resolved in IRAS data). Filled squares: millimeter and IRAS HIRES fluxes. Open triangles: upper limits from Hodapp (1994) K' image (see text).

rower and has a better defined peak near 60 μm . Both distributions, with maxima at FIR wavelengths are characteristic of extremely embedded objects belonging to Class I or Class 0 (Lada 1987, André et al. 1993). A crude estimate of their bolometric temperatures (in the sense of Myers & Ladd 1993) gives approximately 65 K for MMS4 and 55 K for MMS1-2-3, in the boundary between Class 0 and Class I (Chen et al. 1995). Also, the ratio between the bolometric and 1.2 mm luminosities for MMS4 and MMS1-2-3 are 2×10^4 and 4×10^4 , respectively, also in the boundary between Class 0 and Class I (André et al. 1993 define a Class 0 source as one having $L_{bol}/L_{1.3mm} \leq 2 \times 10^4$).

Although higher resolution FIR observations are needed to properly study the status of the individual mm sources, the combination of our bolometer data and the K' image of Hodapp (1994) already suggest that MMS2 is the reddest source of the group. The other mm sources seem to have point-like counterparts at 2.1 μm (although surrounded by diffuse emission see Fig. 1), while MMS2 has only diffuse emission. This, together with the fact that MMS2 is the brightest 1.2 mm source of the group both in peak and integrated intensity (Table 1), suggests that the source is special, and a good candidate for a Class 0 object. The other sources, MMS1, 3, and 4, are most likely Class I (see Sect. 4 for a more complete discussion).

To finish our analysis, we estimate the masses of the dust envelopes of the mm sources using the 1.2 mm emission, which is most likely optically thin. At this long wavelength, radiation is dominated by the cooler, outer part of the envelope, so we make the simplest possible model and assume that the envelopes are isothermal, optically thin dust clouds. We assume a dust temperature of 30 K, in similarity with what is found in the millimeter sources of ρ Ophiuchi (André & Montmerle 1994) and the Orion ridge (Chini et al. 1997a) (if the temperature were 20 K, our masses should be multiplied by 1.6 and if it were 40 K, they should be divided by 1.4). We take a 1.2 mm continuum opacity of $0.01 \text{ cm}^2 \text{ g}^{-1}$, which seems appropriate for Class I and Class 0 objects (e.g., André & Montmerle 1994), and using the fluxes in Table 1, we derive masses of 0.3 , 1.3 , 0.5 , and $0.8 M_{\odot}$ for MMS1, MMS2, MMS3, and MMS4, respectively.

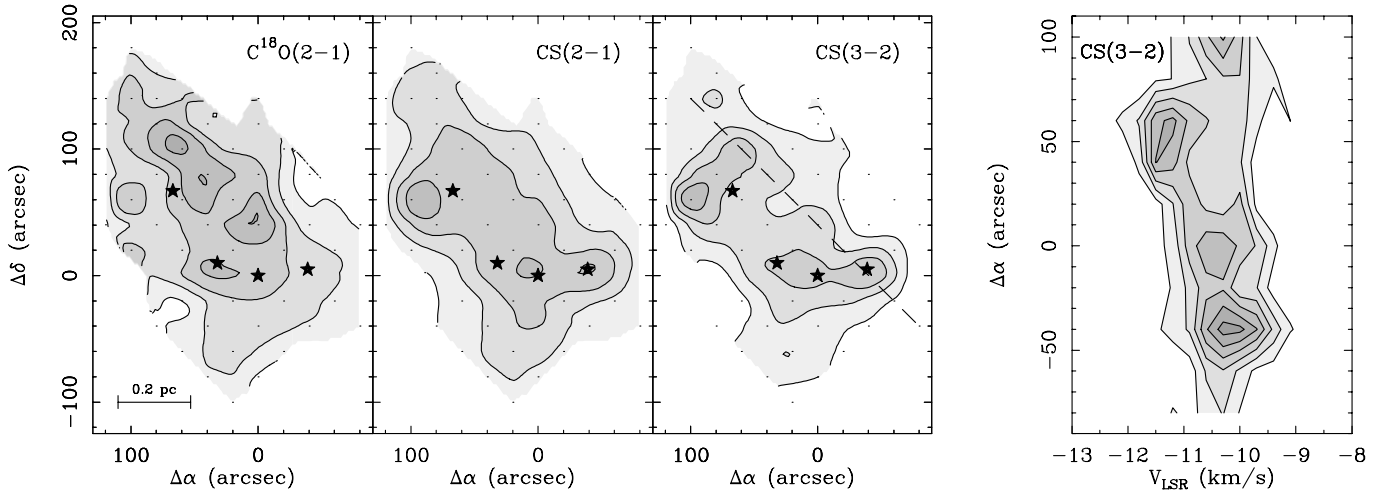


Fig. 3. *Left:* integrated intensity maps for $C^{18}O(2-1)$, $CS(2-1)$, and $CS(3-2)$. For the $C^{18}O(2-1)$, the integrated intensity of a Gaussian fit was used, in order to enhance the signal to noise, while for the CS maps, the emission was integrated directly from the spectra in the V_{LSR} range $-12.5 - 9 \text{ km s}^{-1}$. The filled stars represent the positions of the 1.2 mm continuum peaks (see Fig. 1). Contours are at 2, 4, 6, 8, 10 K km s^{-1} for $C^{18}O(2-1)$, and 1, 2, 3, 4 K km s^{-1} for $CS(2-1)$ and $CS(3-2)$. Offsets referred to $\alpha(1950) = 22^{\text{h}}45^{\text{m}}13^{\text{s}}.5$ $\delta(1950) = 61^{\circ}45'35''$, position of L1211-MMS2. *Right:* $CS(3-2)$ position velocity map along the line shown dashed in the $CS(3-2)$ integrated intensity map. Contours are at 0.4, 0.8, 1.2, 1.6, 2.0, 2.4 K.

3.2. Molecular data

3.2.1. The core

The distribution of dense gas around the mm sources is illustrated by the integrated intensity maps of $C^{18}O(2-1)$, $CS(2-1)$, and $CS(3-2)$ shown in Fig. 3. These maps, made from simultaneous observations, agree well with the ammonia map of Harju et al. (1993) and show that the molecular emission is elongated northeast-to-southwest following approximately the line that connects the mm sources. There is reasonably good agreement between the shapes of the molecular emission and the diffuse mm continuum, indicating that the latter also traces the dense core, but this time in the dust grain component. To illustrate the spectral line shapes, Fig. 4 shows a sample of spectra towards $(-40'', 0'')$ (in the vicinity of MMS1) and $(80'', 80'')$ (in the vicinity of MMS4). CS line widths range from 0.8 km s^{-1} at the narrowest positions to more than 2 km s^{-1} near MMS4. These values are much larger than the thermal velocity component (0.14 km s^{-1} for a 20 K gas), and indicate that in L1211, like in other cores in Cepheus, the velocity dispersion is dominated by supersonic turbulent motions (see also Harju et al. 1993).

We use the $C^{18}O(2-1)$ emission to estimate the core mass because this transition is most likely optically thin and thermalized. Integrating the intensity over the core, we derive a mean $C^{18}O$ column density of $3 \times 10^{15} \text{ cm}^{-2}$, and assuming a $C^{18}O$ abundance of 1.7×10^{-7} (Frerking et al. 1982), we derive a total mass of $150 M_{\odot}$ for an assumed excitation temperature of 20 K (see Sect. 3.2.2). This value of the mass is in reasonable agreement with a virial estimate ($\approx 100 M_{\odot}$) based on the mean $C^{18}O(2-1)$ linewidth of 1.2 km s^{-1} and a mean emission radius of $90''$ (see Fig. 3). It is somewhat larger than the $36 M_{\odot}$ Harju

et al. 1993 derive from NH_3 , as our estimate includes the lower density material not seen in this high density tracer.

Next, we use a large-velocity-gradient analysis to derive densities and column densities from our two CS transitions (e.g., Scoville & Solomon 1974). Given the lack of a well defined core peak, we concentrate on mean parameters over the core by averaging the CS spectra over all positions. In this way, we deduce a mean volume density of $2 \times 10^5 \text{ cm}^{-3}$, a mean CS column density of 10^{13} cm^{-2} , and a mean $CS(2-1)$ optical depth of 0.3. From the ratio of the $C^{18}O$ and CS column densities, and the Frerking et al. (1982) $C^{18}O$ abundance value, we estimate a CS abundance of 6×10^{-10} .

The dense gas in the core has a clear velocity pattern, and this is illustrated with a position-velocity diagram in Fig. 3 (rightmost panel, diagram corresponds to the dashed line in the $CS(3-2)$ integrated map). While most of the gas in the core has a V_{LSR} of about -10.3 km s^{-1} , the gas in the vicinity of MMS4 is blue shifted by about 1 km s^{-1} . As the diagram shows, the shift in velocity does not result from a smooth velocity gradient, but from the presence of a discrete component with $V_{LSR} \approx -11.3 \text{ km s}^{-1}$ near $\Delta\alpha = 50''$. This blue component can be seen in the bottom right spectrum of Fig. 4, and coincides with a relative minimum in the ambient velocity regime, as if the blue gas had been displaced in velocity with respect to the rest of the core. The origin of this displacement is not clear. In Sect. 3.2.2, we will see that MMS4 powers a collimated bipolar outflow, and that the blue outflow lobe lies to the northeast of MMS4, as the brightest blue shifted CS emission does. Thus, it is possible that outflow acceleration causes the dense gas velocity displacement, similarly to what happens in other objects (e.g., Tafalla & Myers 1997). However, there is a significant amount of blue shifted dense gas southwest of MMS4, which goes in opposite direction to the outflow (or at least to the highest velocity

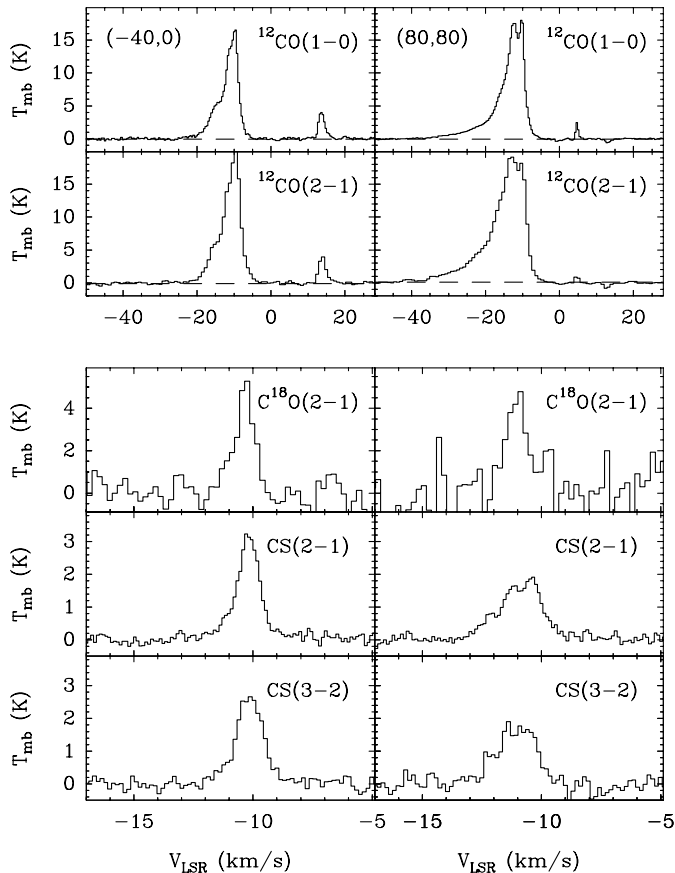


Fig. 4. Spectra toward selected positions. Left panels correspond to position $(-40'', 0)$, which is close to MMS1, and right panels correspond to $(80'', 80'')$, in the vicinity of MMS4. Note blue wings in the CO spectra, indicative of molecular outflow. CO features at $V_{\text{LSR}} \approx 5$ and $\approx 15 \text{ km s}^{-1}$ arise from secondary clouds along the line of sight. Offsets referred to the position of MMS2.

part of it). Furthermore, the amount of momentum in the shifted gas is about $30 M_{\odot} \text{ km s}^{-1}$ (from $\text{C}^{18}\text{O}(2-1)$ data), which is 15 times larger than what we estimate in the outflow (Sect. 3.2.2). If outflow acceleration does not cause the velocity shift, some other mechanism is necessary, as it appears unlikely that the blue gas represents gas superimposed by chance to the hole in the ambient regime.

3.2.2. The outflows

Fukui (1989) reported outflow activity in L1211 but did not present a map of the emission, so we have observed the core in $\text{CO}(1-0)$ and $\text{CO}(2-1)$ to determine the outflow gas distribution. Fig. 5 shows $\text{CO}(1-0)$ velocity maps every 2 km s^{-1} in the velocity range $-22 < V_{\text{LSR}} < -4 \text{ km s}^{-1}$, where most of the emission is concentrated. As the maps show, there is a considerable amount of high velocity blue gas ($V_{\text{LSR}} < -14 \text{ km s}^{-1}$) northeast of MMS4 and southwest of MMS1, and in both cases the distribution is elongated and has the millimeter source near one vertex. At red velocities ($V_{\text{LSR}} > -8 \text{ km s}^{-1}$), the emission is again concentrated towards the vicinity of MMS1 and

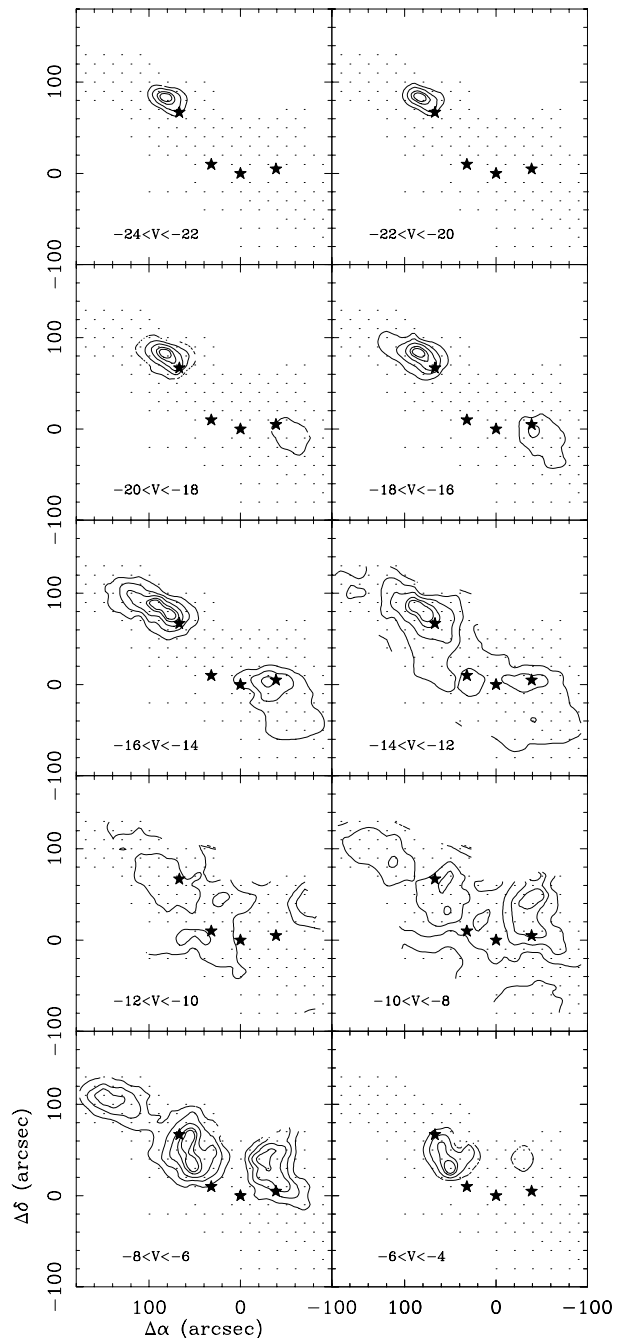


Fig. 5. Maps of $\text{CO}(1-0)$ emission integrated every 2 km s^{-1} over the $-24 < V_{\text{LSR}} < -4$ range. For each panel, contours are at 20, 40, 60, 80, 90% of the map maximum (3.5, 4.7, 6.6, 11.9, 18.4, 32.0, 35.4, 29.8, 8.1, and 3.1 K km s^{-1} for the first, second,... maps, respectively). The high velocity CO emission appears associated to MMS1 and MMS4, and is distributed bipolarly. This is evidence for two molecular outflows emanating from MMS1 and MMS4. The star symbols mark the positions of the MMS sources, and the offsets are referred to the position of MMS2.

MMS4, but this time is located opposite to the blue emission. This bipolar pattern indicates that there are two outflows in the core, one centered on MMS1 and the other on MMS4. These outflows will be referred, hereafter, as the L1211-MMS1 and

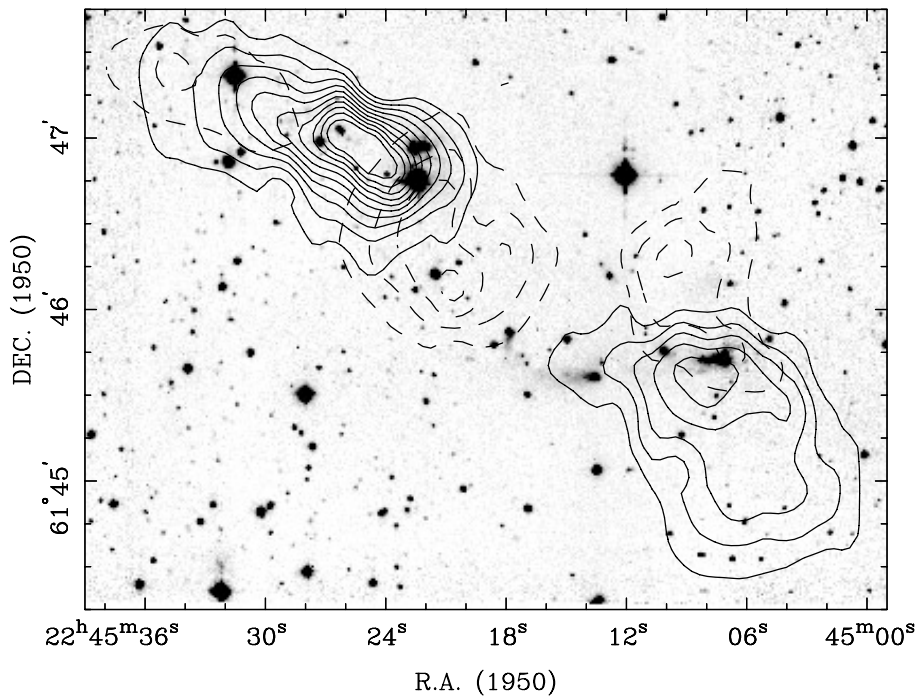


Fig. 6. Maps of the high velocity CO(1–0) emission superposed to Hodapp (1994) K' band image. Note the two bipolar outflows emerging from MMS1 and MMS4. Solid contours represent (blue) emission integrated between -20 and -14 km s $^{-1}$, and dashed contours are for (red) emission integrated between -8 and -2 . Levels are at 3, 6, ... K km s $^{-1}$.

L1211-MMS4 outflows, and their gas distribution is shown in Fig. 6 superimposed on the K' image of Hodapp (1994). CO spectra towards the vicinity of the outflow sources, showing high velocity wings, are presented in Fig. 4

The L1211-MMS4 outflow has a small amount of red emission mixed with the blue lobe near its far end. This mixing of colors suggests that the blue lobe lies almost on the plane of the sky, and that part of its gas appears red because the lobe opening angle is larger than the angle the lobe axis makes with the plane of the sky. A similar situation has been observed and modeled by Cabrit et al. (1988) in B335. The blue gas in the L1211-MMS4 outflow reaches higher velocities than those shown in the velocity maps Fig. 5, and it is still detected up to $V_{\text{LSR}} = -35$ km s $^{-1}$ (see spectrum in Fig. 4), which corresponds to 25 km s $^{-1}$ with respect to the ambient cloud (without any projection correction).

The L1211-MMS1 outflow, on the other hand, seems to have two components with almost orthogonal directions: the large scale lobes extend approximately north-south, while closer to MMS1 ($< 40''$) there is blue shifted gas toward the east and red shifted gas toward the west. This smaller east-west component seems to agree in direction with the small scale optical and K' diffuse emission (Fig. 6), and may indicate that the outflow from MMS1 has in fact four lobes. Quadrupolar outflows have been observed in other systems like IRAS 16293 (Walker et al. 1988) and L723 (Moriarty-Schieven & Snell 1989, Avery et al. 1990), and have been usually interpreted as resulting from the superposition of outflows from unresolved multiple stellar systems (Wootten 1989, Anglada et al. 1991). Our 1.2 mm data do not show any sign of source multiplicity inside MMS1, but Hodapp's higher resolution K' image shows a hint of what may be more than one source embedded in extended emission. High resolution mm observations are necessary to clarify this point.

To estimate the physical properties of the outflows we first estimate the gas kinetic temperature. At ambient velocities, the CO emission is most likely thermalized and optically thick, so the CO peak brightness temperature is a direct estimate of the ambient gas kinetic temperature. In this way, we derive a mean value of 20 K from both CO(1–0) and CO(2–1), which is in good agreement with the 18 K and 17 K values that Wouterloot et al. (1988) and Harju et al. (1993), respectively, derive from ammonia data. For the outflow regime, the CO(2–1)/CO(1–0) line ratios indicate excitation temperatures between 10 and 20 K, depending on the CO optical depth. (A line ratio of 1.4, for example, can either represent optically thin gas at 10 K or gas at 20 K with $\tau_{21} = 2$, see, e.g., Levreault 1988.) As a compromise between these two values, we assume that the outflow gas is at 15 K, and estimate its properties assuming the wing emission is optically thin and in LTE. We take as outflow regime gas velocities larger than 2.5 km s $^{-1}$ with respect to the ambient value (-11.3 km s $^{-1}$ for the L1211-MMS4 outflow and -10.3 km s $^{-1}$ for the L1211-MMS1 outflow), and use a CO abundance of 8.5×10^{-5} (Frerking et al. 1982). In this way, we estimate that the L1211-MMS4 outflow has a mass of $1 M_{\odot}$, a momentum of $5 M_{\odot}$ km s $^{-1}$, and a kinetic energy of 7×10^{44} erg. For the L1211-MMS1 outflow, we estimate about half those values: a mass of $0.5 M_{\odot}$, a momentum of $2 M_{\odot}$ km s $^{-1}$, and a kinetic energy of 2×10^{44} erg. These parameters are in good agreement with what should be expected for outflows powered by sources with a few tens of L_{\odot} (Cabrit & Bertout 1992).

As a final point, we note that the two outflows in L1211 (three, if the L1211-MMS1 outflow is quadrupolar) are not parallel. Fig. 6 shows that the relative angle between the L1211-MMS1 and L1211-MMS4 outflows is about 150 degrees, even without taking into account any additional component along the

third dimension (line of sight). Such non alignment of nearby outflows is also seen in other regions of multiple star forming, like NGC 1333 (Liseau et al. 1988, Langer et al. 1996, Bally et al. 1996, Bachiller et al. 1998), and suggests that whatever the mechanism for outflow orientation is (cloud magnetic field, original gas angular momentum, see, e.g., Shu et al. 1987), it varies over regions of the size of the core, implying a lack of coherence over distances of tenths of a pc or less.

4. Nature of the mm sources and history of star formation in L1211

In Sect. 3.1 we discussed the evolutionary status of the mm sources using their SED, although the lack of spatial resolution of the IRAS data did not allow us to separate some of the components. Here, with the CO data just described, we can refine the above analysis and improve on our conclusions. MMS1 and MMS4 power strong molecular outflows, so their status as YSOs is rather secure. If the typical total duration of the outflow phase is about 2×10^5 yr (Parker et al. 1991), the ages of these sources should be lower than that number.

Comparing the outflow parameters of MMS1 and MMS4 with their mm fluxes, we note that these sources nicely follow the outflow momentum flux vs envelope mass relation found by Bontemps et al. 1996 for a sample of low luminosity outflows (half of them in Ophiuchus). In addition, we note that MMS4 has certain similarities with the Taurus YSO L1551 IRS5, as it has an $L_{bol} = 35 L_{\odot}$ (L1551 IRS5 has an $L_{bol} = 32 L_{\odot}$, Cohen et al. 1984) and very similar molecular outflow parameters when compared with the optically thin numbers given by Moriarty-Schieven & Snell (1989). In addition, if we scale the 1.3 mm flux from L1551-IRS5 (5 Jy, Walker et al. 1990, Ladd et al. 1995, Chini et al. 1997b) to 750 pc, we obtain 175 mJy, close to our MMS4 estimate (see Table 1). We note, however, that both MMS1 and MMS4 are somewhat brighter than the typical Taurus Class I objects (e.g., Kenyon et al. 1993), and this is in agreement with the idea that the turbulent Cepheus cores tend to form stars of higher mass than those formed in the thermally dominated Taurus cores (e.g., Myers & Fuller 1992).

The status of MMS2 is somewhat less clear. In Sect. 3.1, we mentioned that it is associated with strong diffuse $2 \mu\text{m}$ emission, lacks point-like counterpart at this wavelength, and has the largest mm flux, suggesting that it is the youngest source in the group and a good candidate for a Class 0 object. The molecular data, however, do not show evidence for a bipolar outflow, in contrast with other known Class 0 objects (e.g., Bachiller 1996), although high velocity gas is present in its vicinity (Fig. 6). It is still possible, however, that there is an outflow undetected by our observations, as the diffuse K' emission in the image by Hodapp has a cometary shape with a very narrow opening angle, and other Class 0 sources with IR cometary nebulae have outflows filling the nebulae (e.g., L483, see Fuller et al. 1995). If the MMS2 outflow is as narrow as the K' nebula, its emission could have been diluted in our telescope beam and not been detected. We therefore conclude that MMS2 is younger than MMS1 and MMS4, although high sensitivity CO observations are still needed to settle the status of this interesting object.

Finally, the nature of MMS3 is harder to point out as it lacks of outflow or any other clue to its age. It is unlikely it is associated with the optical star in the DSS image (Fig. 1a), as this star has no evidence for diffuse emission and therefore association with dust. It is more likely it is associated with the IR source surrounded by weak diffuse K' emission seen in the Hodapp (1994) image, in which case it would represent a Class I source (i.e., it lacks of visible counterpart). In this case, the source would most likely be older than MMS1 and MMS4, but still a few 10^5 yr old (Myers et al. 1987, Wilking et al. 1989). If it is not associated with any IR source, it may be then a pre stellar condensation, like those found in other clusters (ρ Ophiuchi, see Motte et al. 1998; Serpens, see Testi & Sargent 1998), in which case it would be even younger than MMS2.

If the mm sources in L1211 have at most a few 10^5 yr each, the rate of star formation in the core has been about one star per 10^5 yr in the most recent past. This rate probably has not been maintained for even a few Myr, otherwise a sizable cluster, similar to the stellar density enhancements identified by Chen & Tokunaga (1994) in Orion A, should be present. The K' image by Hodapp shows no obvious clustering apart from the counterparts of the mm sources (see Fig. 6), and the number of K' sources in the image (about 200, Hodapp 1994), is what should be expected for the number of background objects at this wavelength towards the direction of L1211 (Wainscoat et al. 1992). All this suggests, that the beginning of star formation in the core is a rather recent event (a few 10^5 yr).

If the above argument is correct, the L1211 core may be undergoing a period of unusually high star-formation rate. A similar situation has been reported for the Serpens core, where Casali et al. (1993) from mm observations and Hurt & Barsony (1996) from IRAS HIRES data have found an unusually large number of very young stellar objects which can only be explained by a recent burst in star formation (the second in the core history, Casali et al. 1993). Hodapp & Ladd (1995) have also found evidence for rapid formation in cores by using molecular hydrogen emission, suggesting that at least in some cases small stellar groups can form within one outflow life time. Whether rapid star formation is the norm in small stellar groups is still far from clear, but detailed studies of systems like L1211 can shed new light into this intriguing problem.

Acknowledgements. We thank Tyler Bourke and Claudio Codella for sharing with us their unpublished L1211 data, and an anonymous referee for comments and suggestions that improved our presentation. This research has made use of the Simbad data base, operated at CDS, Strasbourg, France, and NASA's Astrophysics Data System Abstract Service. The Digitized Sky Survey was produced at the Space Telescope Science Institute under US Government grant NAG W-2166. MT and RB acknowledge partial support from the Spanish DGES grant PB96-104. PCM acknowledges support from NASA Origins of Solar Systems grant NAG5-6266.

References

- André P., Montmerle T., 1994, ApJ 420, 837
 André P., Ward-Thompson D., Barsony M., 1993, ApJ 406, 122

- Anglada G., Estalella R., Rodríguez L.F., et al., 1991, *ApJ* 376, 615
 Aumann H.H., Fowler J.W., Melnyk M., 1990, *AJ* 99, 1674
 Avery L.W., Hayashi S.S., White G.J., 1990, *ApJ* 357, 524
 Bachiller R., 1996, *ARA&A* 34, 111
 Bachiller R., Guilloteau S., Gueth F., et al., 1998, *A&A* 339, L49
 Bally J., Devine D., Reipurth B., 1996, *ApJ* 473, L49
 Bontemps S., André P., Terebey S., Cabrit S., 1996, *A&A* 311, 858
 Brogière D., Neri R., Sievers A., 1998, *NIC Bolometer Users Guide (IRAM Internal Report)*
 Cabrit S., Bertout C., 1992, *A&A* 261, 274
 Cabrit S., Goldsmith P.F., Snell R.L., 1988, *ApJ* 334, 196
 Casali M.M., Eiroa C., Duncan W.D., 1993, *A&A* 275, 195
 Chen H., Myers, P.C., Ladd E.F., Wood D.O.S., 1995, *ApJ* 445, 377
 Chen H., Tokunaga A.T., 1994, *ApJS* 90, 149
 Chini R., Reipurth B., Ward-Thompson D., et al., 1997a, *ApJ* 474, L135
 Chini R., Reipurth B., Dievers A., et al., 1997b, *A&A* 325, 542
 Cohen M., Harvey P.M., Schwartz R.D., Wilking B.A., 1984, *ApJ* 278, 671
 Crawford D.L., Barnes J.V., 1970, *AJ* 75, 952
 Frerking M.A., Langer W.D., Wilson R.W., 1982, *ApJ* 262, 590
 Fukui Y., 1989, In: Reipurth B. (ed.) *ESO Workshop on Low Mass Star Formation and Pre-Main Sequence Objects*. ESO, Garching, p. 95
 Fuller G.A., Lada E.A., Masson C.R., Myers P.C., 1995, *ApJ* 453, 754
 Guélin M., Zylka R., Mezger P.G., Haslam C.G.T., Kreysa E., 1995, *A&A* 298, L29
 Harju J., Walmsley C.M., Wouterloot J.G.A., 1993, *A&AS* 98, 51
 Hodapp K.-W., 1994, *ApJS* 94, 615
 Hodapp K.-W., Ladd E.F., 1995, *ApJ* 453, 715
 Hurt R.L., Barsony M., 1996, *ApJ* 460, L45
 Kenyon S.J., Calvet N., Hartmann L., 1993, *ApJ* 414, 676
 Kreysa E., 1992, In: *ESA Symposium on Photon Detectors for Space Instrumentation*. ESA, Noordwijk, 207
 Lada C.J. 1987, In: Peimbert M., Jugaku J. (eds.) *IAU Symp. 115, Star Forming Regions*. Kluwer, Dordrecht, p. 1
 Ladd E.F., Fuller G.A., Padman R., Myers P.C., Adams F.C., 1995, *ApJ* 439, 771
 Langer W.D., Castets A., Lefloch B., 1996, *ApJ* 471, L111
 Leveault R.M., 1988, *ApJS* 67, 283
 Liseau R., Sandell G., Knee L.B.G., 1988, *A&A* 192, 153
 Lynds B.T., 1962, *ApJS* 7, 1
 Moriarty-Schieven G.H., Snell R.L., 1988, *ApJ* 332, 364
 Moriarty-Schieven G.H., Snell R.L., 1989, *ApJ* 338, 952
 Motte F., André P., Neri R., 1998, *A&A* 336, 150
 Myers P.C., Fuller G.A.F., 1992, *ApJ* 396, 631
 Myers P.C., Fuller G.A.F., Mathieu R.D., et al., 1987, *ApJ* 319, 340
 Myers P.C., Ladd E.F., 1993, *ApJ* 413, L47
 Parker N.D., Padman R., Scott P.F., 1991, *MNRAS* 252, 442
 Sargent A.I., 1977, *ApJ* 218, 736
 Sargent A.I., 1979, *ApJ* 233, 163
 Scoville N.Z., Solomon P.M., 1974, *ApJ* 187, L67
 Shu F.H., Adams F.C., Lizano S., 1987 *ARA&A* 25, 23
 Tafalla M., Myers P.C., 1997, *ApJ* 491, 653
 Testi L., Sargent A.I., 1998, *ApJ* 508, L91
 Walker C.K., Adams F.C., Lada C.J., 1990, *ApJ* 349, 515
 Walker C.K., Lada C.J., Young E.T., Margulis M., 1988, *ApJ* 332, 335
 Wainscoat R.J., Cohen M., Volk K., Walker H.J., Schwartz D.E., 1992, *ApJS* 83, 111
 Wild W., 1995, *The 30 m Manual: A Handbook for the 30 m Telescope*. IRAM Tech. Rep. 377/95
 Wilking B.A., Lada C.J., Young E.T., 1989, *ApJ* 340, 823
 Wootten A., 1989, *ApJ* 337, 858
 Wouterloot J.G.A., Walmsley C.M., Henkel C., 1988, *A&A* 203, 367
 Yonekura Y., Dobashi K., Mizuno A., Ogawa H., Fukui Y., 1997, *ApJS* 110, 21
 Yu Z.-Y., Nagahama T., Fukui Y., 1996, *ApJ* 471, 867